International Atomic Energy Agency

INDC(CCP)-351
Distrib.: G

INDC INTERNATIONAL NUCLEAR DATA COMMITTEE

The talk presented at International Worskshop
"Fusion neutronics experiments" (Frascati, Italy, 21-22 September 1992)

14MeV FACILITY AND RESEARCH IN IPPE

S.P. Simakov, A.A. Androsenko, P.A. Androsenko, B.V. Devkin,
M.G. Kobozev, A.A. Lychagin, V.V. Sinitca, V.A. Talalaev,
Institute of Physics and Power Engineering,
Obninsk, The Russian Federation

and

D.Yu. Chuvilin, A.A. Borisov, V.A. Zagryadsky
Institute of Atomic Energy,
Moscow, The Russian Federation

July 1993

IAEA NUCLEAR DATA SECTION, WAGRAMERSTRASSE 5, A-1400 VIENNA

Reproduced by the IAEA in Austria
July 1993

INDC(CCP)-351
Distrib.: G

The talk presented at International Worskshop
"Fusion neutronics experiments" (Frascati, Italy, 21-22 September 1992)

14MeV FACILITY AND RESEARCH IN IPPE

S.P. Simakov, A.A. Androsenko, P.A. Androsenko, B.V. Devkin,
M.G. Kobozev, A.A. Lychagin, V.V. Sinitca, V.A. Talalaev,
Institute of Physics and Power Engineering,
Obninsk, The Russian Federation

and

D.Yu. Chuvilin, A.A. Borisov, V.A. Zagryadsky
Institute of Atomic Energy,
Moscow, The Russian Federation

July 1993

The talk presented at International Workshop
"Fusion neutronics experiments" (Frascati, Italy, 21-22 Sept. 1992)

14MeV FACILITY AND RESEARCH IN IPPE.

Institute of Physics and Power Engineering
Obninsk, The Russian Federation

S.P. Simakov, A.A. Androsenko, P.A. Androsenko, B.V. Devkin,
M.G. Kobozev, A.A. Lychagin, V.V. Sinitca, V.A. Talalaev,
D.Yu. Chuvilin, A.A. Borisov, V.A. Zagryadsky

Abstract. Review of experimental facility and research, performed at 14MeV incident neutron energy in the Institute of Physics and Power Engineering, are given. These studies cover the next topics: double differential neutron emission cross sections (DDX), neutron-gamma coincidence experiments $(n,n'\gamma)$ and neutron leakage spectra for spherical assemblies (benchmark). The paper contents description and main parameters of pulsed neutron generator KG-0.3, fast neutron time of flight spectrometer, measuring and data reduction procedures, review of experimental data. Results of experiments are compared with other data; evaluated data files BROND-2, ENDF/B6, JENDL-3; basic theoretical and transport model calculations.

1. Introduction

The development of fission and fusion reactors technologies as well as others applications of radioactivity require the prediction of transport of radiation in the complicated systems and accurate evaluation of induced radiation effects. In particular, the conceptual design of International Thermonuclear Experimental Reactor (ITER), development of Fusion-Fission Hybrid Reactor and others projects are currently underway. This results in the number of neutronics studies of the principal materials and components: first wall, blanket and magnet shield, biological protection, safety etc. [1-4]. Such studies combine the wide variety of differential and integral experiments [5-8].

At the 14MeV pulsed neutron generator KG-0.3 and Time of Flight (TOF) fast neutron spectrometor [9] of Institute of Physics and Power Engineering during the last decade the following experiments and their results analysis have been performed:

- Double Differential Neutron Emission Cross Sections (DDX),

---

*) Institute of Atomic Energy, Moscow, The Russian Federation

- Neutron Inelastic Cross Section (n,n'γ),
- Neutron Leakage Spectra for Spherical Assemblies (benchmark).

The Double Differential neutron emission and (n,n'γ) cross-sections at 14 MeV incident energy, besides the practical importance mentioned above, are rather interesting with basic point of view. From theoretical analysis of energy and/or angular distributions of secondary neutrons the information about different reaction mechanism contributions and excited states parameters could be derived. At 14MeV incident energy (n,2n) and (n,n'γ) reactions contribute practically 100% of non-elastic cross-section for nonfissile nuclei. It is interesting to measure separately the spectra of neutrons and cross sections for these reaction, since the competition between the (n,2n) and (n,n'γ) channels depends on gamma and neutron decay widths at excitation energy of target nucleus just above the neutron binding energy.

In the present work the review of experimental technique, performed measurements, update results and their analyses are presented.

2. Pulsed neutron generator KG-0.3

The basic equipment is a Cockcroft-Walton accelerator with RF electromagnetic discharge ion source and RF deflection and klystron bunching system [9]. The main specifications of neutron generator are listed in Table 1.

The chopping and bunching of an ion beam are carried out before acceleration. At first step the beam is deflected by the sine voltage of 10MHz frequency or 100ns period, thus 20ns length beam pulses pass through the slit. Bunching of the ion clusters are carried out in two-gap buncher system at the same frequency. The buncher compress the ion pulses up to 2ns at target point. To obtain the desired pulse period, the second beam deflecting system is used. The 50ns-width pulses with period equal 2^nx100ns make it possible to pass through diaphragm only first, second, forth ...2^n beam burst.

After high voltage acceleration the deuteron beam passes through analyzing magnet, focusing quadrupole doublet and strikes target. Usually the air cooled TiT targets on Ø11mm Cu backing are

used in the neutronics experiments. About 50cm before the target the pick-up electrode is placed inside the ion drift tube to recieve the stop pulses for TOF analyses.

Table 1. The main parameters of the neutron generator.

Parameter	Value
Sort of accelerated particles	H or D
Maximum acceleration energy	250KeV
Energy of ions extracted from source	30KeV
Maximum current of an ion from source	1mA
Ion pulse width	2.5ns
Pulse height current	0.6mA
Beam spot diameter	5mm
Variable repetition frequency (binary step)	5 to 0.625MHz
Mean beam current (at 1.25MHZ)	1μA
Neutron yield	10^8 1/s

3. Double Differential Neutron Emission Cross Sections (DDX)

3.1. Spectrometer for DDX and (n,n'γ) experiments.

DDX measurements. In the case of DDX measurements the experimental set-up is shown in Fig.1. The measurements have been performed either with short (2-4m) or long (7m) flight paths. In the first case neutron detector is installed in massive shield composed of paraffin-LiH mixture and lead. The direct neutron flux from the target was attenuated by a shadow bar of iron and copper. The advantage of short path is a larger spectrometer aperture (high counting rate) and independence of initial neutron energy versus the scattering angle, since the detector rotates around the scattering sample. The energy resolution in this case is equal 2-1MeV.

To perform the measurement at long flight path (7.1MeV) the neutron detector is installed behind the concrete wall in lead house. Scattering angle is changed by shifting the sample along the detector axis that result in the changing of the incident energy from 14.8 at 30° to 13.4 at 150°. But at this flight path the energy resolution is about two times better (0.6MeV). The later is very important for measurement of the high energy part of neutron emission spectra where energy groups corresponding excitation of discrete levels are appeared. Unfortunately it is impossible do drill the hole in direction perpendicular to

deuteron beam axis and make the incident energy angular independent.

Taking this into account sometimes we combined the measurements at both flight path: low energy part (0.5 - 10MeV) of the spectra at short flight path and high energy (3 - 14MeV) - at long one. The main parameters of experiments are listed in Tab.2.

Table 2. List of (n,xn) and (n,n'γ) experiments.

Experim	Sample	Isotope Abundance	Flight Path, m Short	Long	Detector angle, Step	Ref.
(n,xn)	^{9}Be	100	3.1	7.1	30°-150°, $\Delta\theta$=30°	[10]
	^{52}Cr	99.9	3		30°-150°, $\Delta\theta$=30°	[11]
	^{93}Fe	nature		7.1	30°-150°, $\Delta\theta$=30°	[12]
	^{208}Nb	100		7.1	30°-150°, $\Delta\theta$=30°	[13]
	W	nature		7.1	30°-150°, $\Delta\theta$=30°	[10]
	^{209}Pb	98	3.1	7.1	30°-150°, $\Delta\theta$=30°	[14]
	Bi	100	2.2	7.1	30°-150°, $\Delta\theta$=30°	[14]
(n,n'γ)	^{52}Cr	99.9	2.0		90°	[11]
	^{208}Fe	100	1.7		90°	[15]
	Pb	99	2.2		90°	[14]

Scattered neutrons were registered by a detector consisted of a NE-218 liquid scintillator (Ø10x5cm) coupled with XP-2041 photo multiplier or paraterfenil crystal Ø5x5cm plus photo multiplier Ø3Y-143. The later scintillator has a light output 1.7 times as much as that of NE-218, so detector threshold can be decreased. The minimum detector threshold is about 50keV. The detectors outputs were fed into CAMAC electronic modules connected on line with SM-1420 computer. Anode pulses were used for fast constant fraction timing (start) as well as for gamma-neutron pulse shape discrimination. The overall time resolution of spectrometer is about 3.5ns.

The neutron detector efficiency (Fig.2) was experimentally determined by three methods. In the first one, a miniature designed ^{252}Cf ionization chamber (10^{5}disintegration/s) replaced the sample. Spectrum of prompt fission neutrons was measured by TOF method. The detector efficiency was then reduced from comparison of measured spectrum with standard one [16].

In the neutron energy region above 6MeV, where statistical accuracy with ^{252}Cf source becomes poor, efficiency was measured relative to n-p scattering cross-section [17]. In this case we

placed at the same spot a fast scintillator (stilben crystal Ø1x4cm + PM) detector, that gave the stop pulses for the TOF separation of hydrogen scattered neutrons.

At 14MeV neutron energy the efficiency was measured by associated alpha particle method. In that case the absolute counting of neutron yield from the target was carried out by accumulation the energy spectrum of the associated α-particles with energy 2.9MeV. The silicon surface-barrier (SSB) α-detector was installed in beam tube at 173^{o} to the incident deuteron beam. The calibration of the detector was performed with spectrometric ^{238}Pu α-source with energy 5.7MeV. It is known that SSB-detector efficiency is energy independent, that make this calibration procedure correct.

The absolute normalization factor for converting the neutron spectra to DDX was obtained from comparison with the n-p scattering cross-section (as described above) and by aluminum foil activation method. In the later case Al foils replaced the sample and were irradiated, the target neutron yield been monitoring by Long Counter. The activity of irradiated foils was then measured by β-γ coincidences spectrometer. These data and the standard $^{27}Al(n,\alpha)$ reaction cross-section [17] were used for calculation of the incident neutron flux at the sample position.

The neutron generator pulse mode was controlled by time of flight monitor consisted of fast plastic scintillator СПС-15Б(Ø2x2cm) and FEU-87. The time resolution of this detector was 0.4ns. For monitoring neutron yield from the target and making possible normalization of different runs a Long Counter was used.

(n,n'γ) experiments. The principle of experimental selection of neutrons from (n,n'γ) reaction consists of registration of neutrons in coincidence with the gamma quanta of specific energy. Let us illustrate this for the case of $^{208}Pb(n,n'\gamma)$ reaction (Fig.3). It is known that with 95-99% probability [18], ^{208}Pb excited states feed by gamma cascade the lower 2.61MeV state. Thus the spectrum of neutrons measured in coincidence with 2.61MeV gammas will correspond the $^{208}Pb(n,n'\gamma)$ reaction.

The lay-out of this type experiment is shown in Fig.4. For the detection of gammas we used NaJ(Ø10x10cm) + FEU-141 scintillator

detector. The ring sample had a such size (R=3.8, r=2.5, h=1cm) that to receive the maximum count rate (about 10 true events/hour) and to shield both neutron and gamma detectors from target direct flux by shadow bars.

For $^{208}Pb(n,n'\gamma)$ measurements, the electronics, at first, select gammas from neutrons by time of flight (Fig.3). Then selected events fed amplitude analyzer. Two windows were set up in energy gamma spectrum. The first corresponds the 2.61MeV energy, the second - a little higher. The time of flight spectrum of neutrons coincident with these two windows was recorded in different memory groups as effect+background and background, respectively.

3.2. DDX and $(n,n'\gamma)$ experimental results and comparison with other experiments and evaluated data.

The obtained experimental data are corrected for neutron flux attenuation and multiple scattering in the samples. These corrections were calculated by Monte-Carlo code SSE or BRAND using the evaluated or experimental neutron data. The uncertainties of experimental data include statistics (3-50%), detector efficiency error (5%), absolute normalization (4%) and correction function (3%) errors. Here we demonstrate experimental data for a few elements. The numerical data for elements listed in Tab.2 are available in the papers quoted or on request.

In the neutron emission experiments there is the problem of separation of elastically scattered neutrons. These neutrons were subtracted in the following way. During the experiment the spectrum of neutrons scattered by ^{208}Pb sample was measured. Due to high excitation of the first level (2.7MeV) the elastically and inelastically scattered neutron groups are separated. The ^{208}Pb elastic peak was then fitted to the upper part of elastic peak in the time of flight spectrum of neutrons scattered by heavy mass nuclei.

In the case of light nuclei (e.g. ^{9}Be) the situation is more complicated: elastically scattered neutrons decrease its energy strongly that results in the broadening of the elastic peak. This effect is illustrated in Fig.5, for the reaction $^{9}Be(n,xn)$ at 90^{o}.

The solid line curve is calculated spectrum of neutrons elastically scattered by the beryllium sample. The calculations were done by Monte-Carlo method using SSE code. The multiple elastic collisions, kinematic effects were taking into account to calculate the time of flight spectrum collected in the detector, i.e. the real experimental conditions were simulated. The time of flight spectrum was then transformed to the energy one and folded with the time resolution function of the spectrometer. Finally, the spectrum obtained was fitted to the upper part of elastic peak in the Be neutron emission spectrum. The dashed curves in the Fig.5 are the contributions of single and multiple elastic collisions. It is seen that single elastic scattered neutrons peak have the shape close to $^{208}Pb(n,n_{elastic})$ peak, but multiple elastic scattering contribution changes this shape noticeably.

Beryllium. We compare our measurements with A.Takahashi e.a. data [19]. The agreement is rather good. In the experiment of H.Hogue e.a. [20] the cross-section of inelastic neutron scattering to the 2.43MeV level was measured at 14.94MeV incident energy. The angular distributions of these neutrons compared to our results and ENDF/B6 evaluation are shown in Fig.6 in the center of mass system. It is seen that our data demonstrate less angular anisotropy.

In Fig.7 the angle-integrated cross section is shown. The arrows indicate the level scheme of the ^{9}Be nucleus. It's interesting to notice that only definite states (negative parity) are populated through the inelastic scattering. In this figure experimental results of two our experiments are shown: the data of present one (flight path 7.1m) and of the previous experiment that have been performed at 3.1m flight path. It is seen that increasing of the flight path increase the energy resolution of the spectrometer. This results in to the better separation of the neutron groups, corresponding the excitation of ^{9}Be levels.

Tungsten. In Fig.8 our experimental results are compared with A.Takahashi e.a. experimental [21] and A.Pavlik, H.Vonach compilation [22] data. The agreement is rather good.

The experimental data are compared with ENDF/B6 and JENDL-3 evaluated data as well. It is seen that both files underestimate the emission spectra in 8-13 MeV energy interval. The peak near

14MeV corresponds the inelastic scattering with excitation of low discrete levels (folded with the energy resolution of the spectrometer). It seems that these evaluations contradict the energy behavior of high energy part of the spectrum. Besides, in the JENDL-3 the conjunction of spectra of neutrons from (n,2n) and (n,n') reactions is not correct. All these files do not take into account the angular anisotropy of the inelastically scattered neutrons, that is rather strong for the high energy part of the spectrum.

Chromium-52. The spectrum of neutrons from $^{52}Cr(n,n'\gamma)$ have been measured in [23]. Comparison, performed in [11], indicated that results of both experiments are in reasonable agreement. Our experimental data for (n,xn) and $(n,n'\gamma)$ reactions at 14.1MeV incident energy are compared with ENDF/B6 evaluation (14.5MeV) in Fig.9. It is seen that there is disagreement in high energy part of spectrum.

Lead-208, Bismuth-209. The comparison of DDX from ^{209}Bi is made with data of Pavlik and Vonach [22], who evaluated the data of 4 experiments. The deviation of present experiment results from [22] does not exceed 10%, except the high energy part of spectrum, where data [22] have worse energy resolution. The high energy resolution experimental data of Takahashi e.a. [21] have been measured only at two angles and was not corrected for multiple scattering effects. Discrepancy between our and [19] data somewhere have a value of 50% or more.

The differential neutron emission and inelastic scattering cross-section from pure isotope ^{208}Pb have not been measured previously. These data are compared with ENDF/B6, JENDL-3 and BROND-2 [24] evaluations in Fig.10. It is seen that BROND-2 and JENDL-3 prediction for $(n,n'\gamma)$ shape and absolute value differ much from experimental results.

The energy-angle-integrated cross-sections are listed in Tab.3. Extrapolation of cross-section below the detector threshold was made using the models calculations described below. It is seen that agreement of integrated cross section is better than the differential one. Nevertheless BROND-2 and ENDF/B6 underestimate $^{208}Pb(n,2n)$ and JENDL-3 overestimate $^{208}Pb(n,n'\gamma)$ cross-sections.

Table 3. Comparison of neutron production cross-sections (mb) at 14.1MeV.

Nucleus	Reaction	experiment	BROND-2	ENDF/B6	JENDL-3
^{52}Cr	(n,xn)	1443 ± 120		1510	1375
	(n,n'γ)	907 ± 80		907	721
	(n,2n+nα)	537 ± 45		603	654
	(n,nα)			45	96
^{56}Fe	(n,xn)	1732 ± 140	1605	1638	1726
	(n,n'γ)	704 ± 70	676	756	743
	(n,2n+nα+np)	1028 ± 95	929	882	983
	(n,nα+np)		63	51	77
^{208}Pb	(n,xn)	5165 ± 300	4413	4579	4867
	(n,n'γ)	405 ± 30	461	411	589
	(n,2n)	2380 ± 140	1976	2084	2139
^{209}Bi	(n,xn)	5220 ± 310	4857		4773

3.3 Theoretical calculations and analyses of experimental results

The theoretical approaches will be demonstrated for the case of two adjacent nuclei: ^{208}Pb and ^{209}Bi. ^{208}Pb is a double-closed-shell nucleus, on the other hand the neighboring element ^{209}Bi has a valence protons in $h_{9/2}$ shell. It is known that a few low lying levels in ^{209}Bi can be described in the model of weak coupling of valence proton with the vibration states in magic core ^{208}Pb, but others levels - as single particle/hole transitions [25]. The comparison of neutron experimental spectra from ^{208}Pb and ^{209}Bi can give the information about what kind of states populated in neutron non-elastic reactions, the validity of weak coupling model and energy dependence of level density function.

The reaction cross-sections were calculated in the framework of compound and direct mechanisms. The statistical part of reaction was calculated using Hauser-Feshbach model, including angular momentum and parity conservation, competition between neutrons, gammas and charge particles emission. We calculated neutron emission coefficients with optical model potential of Rapaport e.a. [26] for lead and of Lawson e.a. [27] for bismuth. The transition to the discrete levels of residual nuclei was taken into account. For example: 20 states till the excitation energy

U=4.2MeV for the ^{208}Pb and 40 states till U=3.6MeV for ^{209}Bi [18]. At the higher excitation energies level density function, that takes into account shell, superfluid and collective effects [28], was used. The radiation strength functions for Eλ and Mλ transitions, influenced on the gamma-neutron competition, were calculated in Axel-Brink model. They absolute normalization corresponds the experimental observed radiation width at neutron binding excitation energy [29].

The direct neutron inelastic scattering cross-section was estimated using a coupled-channel model and distorted wave Born approximation. Form-factors of the direct transitions were calculated in Bohr-Mottelson model for collective excitation modes. The excitation energies, deformation parameters of vibration states in ^{208}Pb was taken from the similar analyses of ^{208}Pb(p,p') reaction [30,31]. The same parameters was taken for ^{209}Bi (the model of weak coupling $h_{9/2}$ proton with vibration states of magic core ^{208}Pb).

The experimental angular-integrated neutron emission spectra for ^{208}Pb and ^{209}Bi are shown in Fig.11. These spectra practically coincide each other in the whole energy region (the ratio of ^{209}Bi cross-section to ^{208}Pb one is shown in the insert of Fig.11). The angular distributions of secondary neutrons agree for these two nuclei as well.

Therefore, from the comparison of DDX we can make conclusion that adding of one proton to closed-shell ^{208}Pb does not influence on energy/angle distributions of secondary neutrons. What does it mean with physical point of view ? We can receive the answer after comparison of experimental and calculated data.

Such comparison is shown in Fig.12. It is seen that compound component describes the low-energy part of spectra. The agreement of spectra from both nucleus means the equal energy dependence of level density functions for the residual nucleus. The direct component contributes to the high energy part and satisfactory describes the excitation of the first 3^- state. Thus we can make conclusion that in direct inelastic scattering only the collective states are practically excited, and weak coupling model is a good approximation for the ^{209}Bi.

In the intermediate energy region the theoretical model

calculation underestimate experimental DDX. The difference between experimental spectra and compound one is estimated to be 350mb, whereas the total direct cross-section equal 210 mb. The remained part (40%) of nonequilibrium process can result from missed in calculation collective or single particle states, or from more complicated multi-step processes.

The spectrum of neutrons from reaction $^{208}Pb(n,n'\gamma)$ is shown in Fig.12. For neutron energies above E_{n2n}=6.64MeV (maximum energy from (n,2n) reaction) the spectrum of inelastically scattered neutrons have to coincide with the emission neutron spectrum. In lower energy region (when excitation of ^{208}Pb after the emission of first neutron exceeds the neutron binding energy) the contribution of neutrons from $(n,n'\gamma)$ and (n,2n) reactions becomes energetically possible.

It is interesting to notice that $(n,n'\gamma)$ spectrum sharply decrease with decreasing of neutron energy at 5Mev but not at E_{n2n}. In Fig.12 it is seen that this critical point corresponds the possibility of population of high spin isomeric level $13/2^+$ (U=1.68MeV) in reaction $^{208}Pb(n,2n)^{207}Pb$. This effect can be described if one take into account the total spin conservation law. The high orbital momentum (about 12/2), input by 14MeV neutron, can not be compensated by two neutrons with total energy less or equal E_{n2n}. Therefore $^{208}Pb(n,2n)$ reaction will populate with higher probability the high spin states.

These qualitative explanation is confirmed by statistical model calculation, in which the gamma-neutron competition and spin conservation law are taken into account. Since the sum of compound and direct cross-section underestimates the experimental one in energy region under interest, we introduced precompound emission of the first neutron. As can be seen in Fig.12, the spectrum of inelasticaly scattered neutrons is satisfactory described. It is interesting to notice that reaction $^{208}Pb(n,n'\gamma)$ with 20% probability results in population of unbound states in ^{208}Pb. It means that sum energy of gammas from this reaction have to be about 0.7MeV larger in comparison with case when gamma competition is absent. We would like to notice that ENDF/B6 evaluation (distributed at the same time when our data have been published [14]) predicts $(n,n'\gamma)$ spectrum very well (see Fig.10)

4. Neutron leakage spectra

4.1 Benchmark experiments.

We have made the time of flight measurements of neutron leakage spectra from sphere piles with T(d,n) and Cf sources. These experiments are similar except the sources. The parameters of the shells investigated are listed in Tabl.4. The hole in the sphere is used for input of neutron source. Preliminary experimental results were published in [32], final - in [33], numerical data are available on request.

Table 4. Parameters of the shells and experiments.

Source	Element	Radius, cm		Wall thickness		Hole Ø, cm	Concentration, 10^{22} cm^{-3}	Angles, ^{o}	Target
		out.	inn.	cm	mfp*				
	Be	11	6	5.0	0.9	5.0	12.36	0,30,60	a
	Al	12	4.5	7.5	0.6	6.2	5.966	0,40,75	b
	Fe	12	4.5	7.5	1.7	6.2	8.374	0,40,75	a
	Ni	12	4.5	7.5	1.7	6.2	9.016	0,40,75	b
T(d,n)	Pb	12	4.5	7.5	1.7	5.0	3.30	0,30,60	a
	LiPb	20	6	14.0	2.2	5.0	2.76-Pb, 0.565-Li	40	b
	Bi	12	3	9.0	1.4	5.0	2.82	0,60,95	a
	U	12	4	8.0	2.2	5.0	4.76-^{8}U, 0.019-^{5}U	0,60,95	a
	Th	13	3	10.0	1.7	5.0	2.93	0,60,95	a
^{252}Cf	U	12	4	8.0	2.8	5.0	4.76-^{8}U, 0.019- U^{5}		
	Th	13	3	10.0	2.1	5.0	2.93		

* - sphere wall thickness in mean free path units of 14MeV neutrons or mean energy of Cf fission neutrons.

14MeV Experiment. Experimental set up is shown in Fig.13. Source assembly design with Ø28mm TiT target is shown in Fig.14 (insert "a"). The angular distribution of source neutron yield was measured by: i). Simultaneous irradiation of ten Al foils, located at 10 cm distance around the target, and counting the induced activity of ^{24}Na by the β-γ technique; ii). Measuring of the neutron yield by TOF method. In the last case the angular resolution (about 1^{o}) was sufficient to measure the narrow deep close to 90^{o}. To decrease this attenuation we became use more upgrading source design with Ø11mm TiT target inside thin Al holder (insert "b").

The leakage spectra from the shells were measured by

scintillator detector at 3.7m flight path. The background was measured with 1m long iron shadow bar, the number of source neutron was determined by measuring α-associated particles.

^{252}Cf experiment. The geometry of benchmark experiment with ^{252}Cf neutron source is shown in Fig.15. The fast ionization chamber with ^{252}Cf, that gives the stop pulses for TOF analysis, was installed in the shell center. The intensity of source was about 5×10^{5} n/sec. The chamber was fabricated rather miniature (Ø20×0.18mm electrodes, 0.35mm wall thickness), that results in small corrections (1-3%) for the standard Cf neutron fission spectrum.

The flight path was 3.85m, the time resolution - 3ns. The total number of source neutrons during experiment was obtained by counting the ^{252}Cf fission fragments and using known value of prompt fission neutrons ν=3.77661 [34].

Stability and experimental errors. In benchmark experiments the problem of equipment stability and experimental errors is of high importance: the data should be obtained with as high precision as possible. The main parameters of spectrometer (detector efficiency, absolute normalization factor etc.) were measured several times during one experiment, thus the stability of apparatus were controlled and overall errors were decreased. The estimated errors of experimental data and main components are listed in the Tab.5. These errors include the uncertainty of standard cross-sections [16,17] as well as the deviations of different runs during the calibrations and measurements.

Table 5. Uncertainties of experimental data.

Components	Value
Statistics	1 - 4 %
Absolute normalization	3%
Detector efficiency	5%
Correction calculation	2%
Total	6 - 7%

4.2 Corrections for nonspherical effects and measuring procedure.

Some transport codes use one-dimensional (spherical) approximation. In this case the comparison of the calculations is possible only with the results of ideal spherical benchmark experiment. In practice, however, there are factors that violate this symmetry and could brings other perturbation:

- -the hole (channel) in the shell assembly for input neutron source;
- -angular anisotropy of source neutrons and energy distortion by target assembly;
- -time of flight spectrometry with bulk samples.

Therefore before the comparison, the experimental data have to be corrected for. It was done using three dimensional code BRAND [35].

The channel in the spherical assembly was 5-6.2cm in diameter (Tab.4) that correspond the removed material about 2-2.5% of total shell weight. The correction have to be the same order but could be energy depended, thus we introduce correction function as a ratio of leakage spectra calculated for shells without and with channel: $C_1(E)=L(E)/L_c(E)$.

In the time of flight method the neutron energy is strictly connected with the distance between sample and detector and flight time only for the infinitely small sample. In benchmark experiments the size of assembly is not negligibly small: ratio of sphere radius to flight path is about 3% that could result in some correction. To evaluate it value we simulate by Monte-Carlo method the time of flight benchmark experiment and data reduction procedure. The calculations take into account the experiment geometry, neutron detector efficiency and the real travel time, that neutron spent on the way source-sphere-detector. The evaluated correction function is determined as $C_2(E)=L(E)/L_T(E)$, where $L_T(E)$ - leakage spectrum calculated by time dependent Monte-Carlo technique.

Angular-energy distribution of source neutrons. In the benchmark studies it is rather important to know the angular distribution and energy spectrum of the source neutrons. The source holder and other surrounding materials can change the

energy-angular distribution of neutron producing reaction.

a). The angular distribution of ^{252}Cf fission neutrons is originally isotropic, energy spectrum $S_{Cf}(E)$ is known with 3-5% uncertainty in the energy region 0.1-10MeV [16]. Due to inelastic scattering of Cf-neutrons on chamber constructional materials, the energy spectrum of neutron source $S_S(E)$ will have slightly different shape $S_S(E)$, thus correction function $C_3(E)=S_S(E)/S_{Cf}(E)$ have to be calculated.

b). The T(d,n) reaction yields 14MeV neutrons with slight forward anisotropy - see long dashed curve [36] in Fig.14. In our first experiment we used Ø28 mm targets. In that case there is 20% attenuation of neutron yield at angles close to 90^o, that results in 4% correction in the whole solid angle 4π. The calculations (solid curve) prove that these distortions result from the neutron nonelastic interaction with target assembly. To reduce this effect we became use the Ø11mm targets in thin Al holder (insert "b"). The calculated angular distribution in that case is indicated by the short dashed curve, the total attenuation is equal now to 2.5%.

The energy spectrum of source neutrons is shown in Fig.18. It is seen that 14MeV neutron peak has a low energy (5-10MeV) tail, results presumably from source neutrons interaction with collimator wall, and broad low energy (0.2-5MeV) bump. The later is caused by nonelastic scattering of 14MeV neutrons on the target assembly. It is interesting to notice that contribution of these neutrons (2.5%) in the target energy spectrum is approximately equal to the attenuation factor obtained in the target neutron angular distribution study.

The total correction function $C(E)=C_1(E)\times C_2(E)\times C_3(E)$ and their components are shown in Fig.16 (U sphere, ^{252}Cf neutron source) and Fig.17 (Bi,T(d,n) source). It is seen that corrections are energy dependent and has the values up to 6-10%, that exceed the experimental uncertainty, thus measured neutron leakage spectra have to be corrected for: $L_{true}(E)=L_{raw}(E)\times C(E)$.

4.3 Comparison with transport calculations.

Calculation of neutron leakage spectra from sphere assembles

have been performed with three dimensional Monte Carlo code BRAND [35] and one dimensional code ANISN. The neutron data were taken from ENDF/B6, JENDL-3 and/or BROND-2 evaluated data libraries.

In BRAND code the pointwise data files are used directly (without converting to multigroup form). The problem of simulating the transport of neutrons in the unresolved resonances energy region is solving now. This is the reason why the calculation made with BRAND is restricted by low energy limit (usually about 1MeV). The energy-angular distribution of T(d,n) source was taken from [36] (see long dashed curve in Fig.14). To take into account the spectrometer energy resolution and neutron flux attenuation of target holder the calculated spectra were folded with measured energy spectrum of neutron from the target (source). The effect of this procedure is the following: the 14MeV peak becomes broader and valley in the spectrum around the 8MeV is filled.

Calculation with ANISN were performed in P5/S16 approximation, the radius step was about 2mm. The evaluated data libraries were processed to 28-group format [37] using code GROUCON [38]. Weight function has a shape of Fermi spectrum (1/E) for energy less than 2.5MeV, fission spectrum - in region 2.5-14MeV and energy independent - for higher energy. This is standard procedure for generation 28-group library [37], intensively used for fission reactor calculations. The main goal of theses calculations was the investigation of uncertainty of 28-group presentation of evaluated data. In this calculations the energy distribution of source neutrons was obtained from measured one.

The experimental and calculated leakage neutron spectra for the spheres are shown in Figs.18-21 and their ratios (C/E) are listed in Tab.6.

In the previous works [32] we made comparison with ENDF/B4 and JENDL-2 libraries (75-groups format), using one dimensional Monte Carlo transport code BLANK [39]. These results are listed in Tabl.6 as well.

In the lower energy region of leakage spectrum (0.1-1MeV) the resonance like structure manifests itself in both experimental and calculated data. The analyses indicates that bumps in leakage spectra correlate with valleys in total cross-sections and vice versa (see Fig.19, where σ_{tot} for Al is shown by dashed line).

It is interesting to compare experimental data with data received in other laboratories. It was done for AL and Ni spheres. The neutron leakage spectra was measured for Al sphere of the same sizes in [40], but using pulse height method and scintillator detector. It is seen (Fig.19) that these data has unreal oscillations.

At OKTAVIAN spectrometor leakage spectra was measured for Ni sphere (R=16, r≅2.5cm). Since the sizes are different, the direct intercomparison is impossible. We compared the ratios of experimental data to transport calculation with ENDF/B6 for both spheres(Fig.22). It appears that energy shapes of C/E are similar, but the ratios are shifted on scaling factor ≅1.5. Possibly it means that in one or both experiments the absolute normalization (e.g. source strength or detector efficiency) was done incorrectly. It is strange that C/E ≅ 1.4 for 14MeV group in experiment [6]. We estimated transmission of the spheres according the simple formula $T = \exp(-\Sigma_{nonel} \times (R-r))$, where Σ_{nonel} is macroscopic nonelastic cross section at 14.1MeV neutron energy and (R-r) - wall thickness of the sphere. The ratio T(ENDF/B6)/E is about 25% grater than with transport code calculations, but for the data of [6] this ratio nevertheless equal 1.7 (see Fig.22).

From analyses of the data presented in the Tabl.6 and Figs.18-22, the following conclusions can be derived:

-Discrepancies between predictions of updated evaluated data libraries (BROND-2, ENDF/B6 and JENDL-3) are about a few percent in low energy part of leakage spectra E < 1-2MeV and - at E = 14MeV. In the intermediate energy region the discrepancies achieve a value of tens or even hundred percents. (See calculations with ANISN).

-28-group format for evaluated data results in additionally 10-20% errors. (Compare ANISN and BROND results with ENDF/B6).

-Remark on ENDF library evolution: comparison of ENDF/B4 and ENDF/B6 predictions reveals that agreement with experimental data becomes better in the most of energy groups for late version. (Compare BRAND and BLANK results with different versions).

-Only for Al sphere the transport calculations with ENDF/B4 practically agree with experimental results in energy bins, taking into account the errors quoted.

-In the case of Be we compared experimental (present work) and evaluated (ENDF/B6) data for angular-integrated neutron emission cross section at 14.1Mev incident energy (Fig.18). It is seen that evaluation overestimate spectrum of secondary neutron, this results in the overestimation in the benchmark experiment as well. Therefore, knowledge DDX is very useful for understanding the discrepancies in the integral experiments.

-In low energy range the transport calculations underestimate experiment.

-The general conclusion: the disagreements need additional experimental data intercomparison, transport calculations, joint analyses of integral and differential data. This is in progress now.

Table 6. Ratio of calculated to experimental data (C/E).

Sph-	Energy	ANISN (28-group)			BRAND	BLANK	
ere	MeV	BROND-2	ENDF/B6	JENDL-3	ENDF/B6	ENDF/B4	JENDL-2
	0.4- 0.8	0.77±.06			0.77±.06	0.81±.05	
	0.8- 1.4	0.84±.06			0.87±.06	0.75±.06	
	1.4- 2.5	1.34±.09			0.98±.07	0.94±.07	
Be	2.5- 4.0	1.43±.10			1.11±.08	1.04±.07	
	4.0- 6.5	1.28±.09			1.23±.09	1.45±.10	
	6.5-10.5	0.96±.07			1.13±.08	1.23±.08	
	10.5-15.0	0.89±.06			0.96±.07	0.84±.06	
	0.2- 0.4		0.76±.06	0.76±.06		1.04±.07	
	0.4- 0.8		0.67±.05	0.69±.05		0.92±.06	
	0.8- 1.4		0.79±.06	0.79±.06		0.94±.07	
	1.4- 2.5		0.88±.06	0.88±.06		0.96±.07	0.85±.06
Al	2.5- 4.0		0.83±.06	0.80±.06		0.90±.06	0.82±.06
	4.0- 6.5		0.85±.06	0.73±.06		0.97±.07	0.80±.06
	6.5-10.5		0.87±.06	0.78±.06		1.03±.07	0.85±.06
	10.5-15.0		0.93±.06	0.97±.07		0.91±.06	1.02±.07
	0.2- 0.4	0.79±.06	0.79±.06				
	0.4- 0.8	0.73±.06	0.71±.06				
	0.8- 1.4	0.85±.06	0.89±.06				
Fe	1.4- 2.5	0.92±.06	0.95±.07			0.97±.07	1.15±.09
	2.5- 4.0	0.97±.07	1.01±.07			0.92±.06	1.14±.08
	4.0- 6.5	0.99±.07	0.85±.06			0.98±.07	0.88±.06
	6.5-10.5	1.13±.08	0.87±.06			1.30±.09	0.80±.06
	10.5-15.0	0.78±.06	0.84±.06			0.82±.06	0.87±.06
	0.2- 0.4	0.52±.04	0.90±.06			0.71±.06	
	0.4- 0.8	0.72±.06	0.91±.06			0.69±.05	
	0.8- 1.4	0.77±.06	0.88±.06		0.78±.06	0.79±.06	
Ni	1.4- 2.5	0.90±.06	0.85±.06		0.68±.05	0.85±.06	1.01±.07
	2.5- 4.0	0.75±.05	0.79±.06		0.75±.06	0.71±.05	1.10±.08
	4.0- 6.5	0.64±.05	0.81±.06		0.91±.06	0.74±.05	0.96±.07
	6.5-10.5	0.64±.05	0.80±.06		0.95±.07	1.14±.08	0.80±.06
	10.5-15.0	0.92±.06	0.86±.06		0.90±.06	0.90±.06	0.94±.07

Table 6.(contined)

Sphere	Energy MeV	ANISN (28-group) BROND-2	ANISN (28-group) ENDF/B6	ANISN (28-group) JENDL-3	BRAND ENDF/B6	BLANK ENDF/B4	BLANK JENDL-2
	0.4- 0.8	0.70±.05	0.66±.05	0.72±.05		0.89±.06	
	0.8- 1.4	0.78±.06	0.74±.05	0.80±.06		0.93±.07	
Pb	1.4- 2.5	0.80±.06	0.81±.06	0.88±.06	0.86±.06	0.83±.06	
	2.5- 4.0	0.74±.05	0.95±.07	1.10±.08	0.93±.07	0.90±.06	
	4.0- 6.5	0.44±.03	0.88±.06	0.84±.06	0.91±.07	0.90±.06	
	6.5-10.5	0.37±.03	0.85±.06	0.84±.06	1.05±.07	0.93±.07	
	10.5-15.0	1.22±.09	1.16±.08	1.10±.08	1.16±.08	1.00±.07	
	0.2- 0.4	0.64±.05	0.69±.05	0.67±.05		0.83±.06	
	0.4- 0.8	0.73±.05	0.68±.05	0.76±.06		0.85±.06	
	0.8- 1.4	0.73±.05	0.68±.05	0.75±.06		0.74±.05	
Li	1.4- 2.5	0.82±.06	0.83±.06	0.89±.07		0.71±.05	
Pb	2.5- 4.0	0.80±.06	1.03±.07	1.14±.08		0.81±.06	
	4.0- 6.5	0.40±.03	0.93±.07	0.89±.06		0.97±.07	
	6.5-10.5	0.19±.02	0.64±.05	0.56±.05		1.02±.07	
	10.5-15.0	1.34±.09	1.24±.09	1.17±.08		1.06±.07	
	0.4- 0.8					1.09±.07	
	0.8- 1.4					1.32±.09	
U	1.4- 2.5					1.31±.09	
+	2.5- 4.0					1.39±.10	
14	4.0- 6.5					1.28±.09	
	6.5-10.5					0.86±.06	
	10.5-15.0					1.08±.08	
	0.4- 0.8	0.71±.05		0.68±.05		1.04±.07	
	0.8- 1.4	1.14±.08		0.92±.06		1.08±.08	
U	1.4- 2.5	1.06±.07		0.99±.07		1.05±.07	
+	2.5- 4.0	0.95±.07		1.00±.07		1.07±.07	
Cf	4.0- 6.5	0.92±.06		0.95±.07		1.09±.08	
	6.5-10.5	0.71±.05		0.73±.05		1.23±.09	
	10.5-14.0	0.24±.02		0.23±.02		0.68±.05	

References

1. World Request List for Nuclear Data. INDC(SEC)-88/URSF, IAEA, Vienna, 1988
2. E.T.Cheng. Proc.Int.Conf.on Nuclear Data for Science and Technol., May/June 1988, Mito, Japan, p.187, Saikon, Tokyo(1988)
3. J.J.Schmidt. Acta Physica Hungarica, 1991, v.69, p.269
4. FENDL-2 and associated benchmark calculations. (Ed.A.B.Pashchenko and D.W.Muir) Report INDC(NDS)-260, Vienna, 1992
5. L.F.Hansen e.a. Nucl.Sci.Eng. 1986, v.92, p.382; 1976, v.60, p.27; 1973, v.51, p.278; 1979, v.72, p.35; C.Wong e.a.:UCRL-51144(1971); UCRL-91774(1985)
6. S.Iwasaki e.a. Ibid 2, p.229;
   C.Ichihara e.a. Report JAERI-M91-062, p.255
   Y.Yanagi e.a. Report A84-02(1984);A84-04(1984)
7. D.Albert e.a. ZFK-562, Dresden, 1985, p.85
   T.Elfruth e.a.:Kerntechnik, 1990, v.55, p.156; 1987, v.49, p.121
   О.В.Баранов и др.:Вопросы атомной науки и техники. Сер:Ядерн.константы, вып.1, 28(1990)
8. И.Г.Горячев и др.Интегральные эксперименты в проблеме переноса ионизирующих излучений. М.Энергоатомиздат. 1985

9. А.Б.Ануфриенко и др.:Вопросы атомной науки и техники.Серия Реакторостроение,5(19),с.11(1977)
10. S.P.Simakov, B.V.Devkin e.a. Proc. of IAEA CRP Meeting, Thailand, 31 March-2 April 1992. Report INDC, Vienna, 1992
11. S.P.Simakov, A.A.Lychagin, e.a. Nucleon Induced Reaction. Institute of Physics, Bratislava, 1988, v.15, p.266; A.A.Lychagin, S.P.Simakov e.a. Ibid, p.272.
12. L.A.Lychagin, V.P.Lunev e.a. Nuclear Data for Scince and Technology, Mito, 1988, p.307
13. Л.А.Лычагин, В.А.Виноградов и др.Атомная энергия, 1984, т.57, с.266
14. S.P.Simakov, B.V.Devkin e.a. Report INDC(CCP)-315/L, IAEA, Vienna, 1990
15. Л.А.Лычагин, С.П.Симаков и др. Ядерная физика, 1987, т.45, с.1226
16. W. Mannhart. Report IAEA-TECDOC-410, Vienna, 1987, p.158
17. Data Standards for Nuclear Measurements. Report IAEA-TECDOC-227, IAEA, Vienna, 1983
18. C.M. Lederer, V. Shirtley. Tables of Isotopes. New York, 1978
19. A.Takahashi, J.Yamamoto e.a. Oktavian Report A-87-01, Osaka, 1987
20. H.H.Hoque, P.L.Von Behren e.a. Nucl.Sci.Eng., 1978, v.68, p.38
21. A.Takahashi, Y.Sasaki e.a. Report JAERI-M89-214, Tokio, 1989
22. A.Pavlik and H.Vonach. Physics Data, Karslruhe, 1988
23. S.Hlavach, P.Oblozincky e.a. Nucleon Induced Reactions. D.Reidel Publishing Company, 1986, p.298
24. Библиотека рекомендованных оцененнх ядерных данных БРОНД-2. Вопросы атомной науки и техники. Серия Ядерные константы, 1991, вып. 2-3
25. W.T.Wagner e.a. Phys. Rev., 1975, v. C12, p. 757
26. J.Rapaport e.a. Nucl. Phys., 1979, v. A330, p. 15
27. R.D.Lawson e.a. Phys. Rev., 1987, v. C36, p. 1298
28. О.Т.Грудзевич и др. Нейтронная физика. М.ЦНИИАИ.1988, т.2, с.96
29. В.М.Бычков и др. Вопросы атомной науки и техники. Сер.Ядерные константы, 1987, вып. 3, с.14
30. W.T.Wagner e.a. Phys. Rev., 1975, v. C11, p. 486
31. P.H.Stelson e.a. Nucl. Phys., 1965. v. 68, p. 97
32. S.P.Simakov e.a. Report on FENDL Meeting, Vienna, November 1991; A.A.Androsenko e.a. Kernenergie, 1988, v.31, p.422; Proc.Int.Conf. on Neutron Physics, Sept 1988, Kiev, USSR, v.3, p.194, Moscow, 1988; S.P.Simakov e.a. Report ZFK-646, Gaussig, 1988, p.111
33. S.P.Simakov, A.A.Androsenko e.a. Proc.of 17 Simp.on Fusion Techn., Rome, 14-18 Sept 1992.
34. E.J.Axton e.a.:Nucl.Sci.Techn.5,609(1984)
35. А.А.Андросенко, П.А.Андросенко. Вопросы атомной науки и техники Серия: Физика и техника ядерных реакторов, 1985, вып.7, с.33
36. J.Csikai, Zs.Lantos e.a. IAEA-TECDOC-410, Vienna, 1987, p.296
37. Л.П.Абагян, Н.О.Базазянц и др.:Групповые константы для расчета реакторов и защиты. М., Энергоиздат, 1981
38. В.В.Синица, А.В.Ринейский Вопросы атомной науки и техники. Серия Физика ядерных реакторов. 1989, вып.2, с.30
39. С.Марин, Д.В.Марковский и Г.Е.Шаталов. Препринт ИАЭ-2382, Москва, Институт атомной энергии, 1977
40. А.А.Борисов, В.А.Загрядский, Д.Ю.Чувилин, М.Пулпан и др. Препринт ИАЭ-4990/8, Москва, Институт атомной энергии, 1989

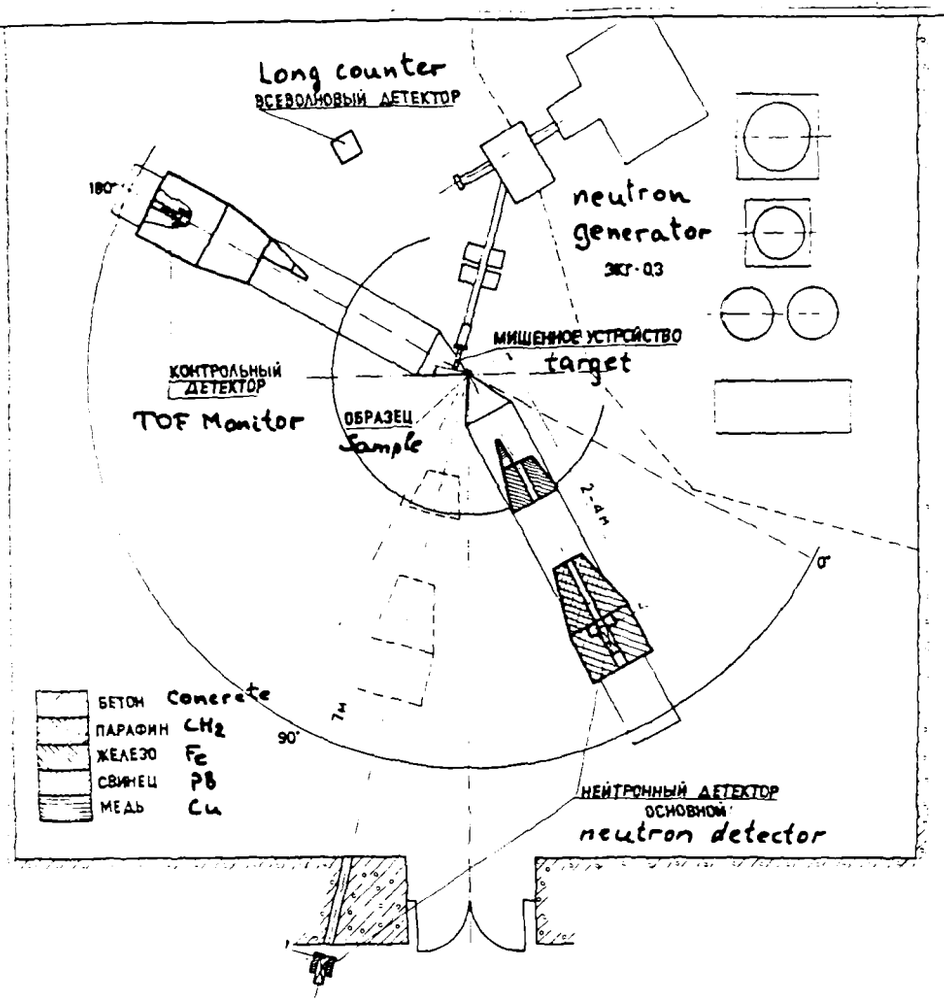

Fig. 1. Lay-out of experiment for measuring the neutron emission spectra at short (2 - 4m) and long (7m) flight path.

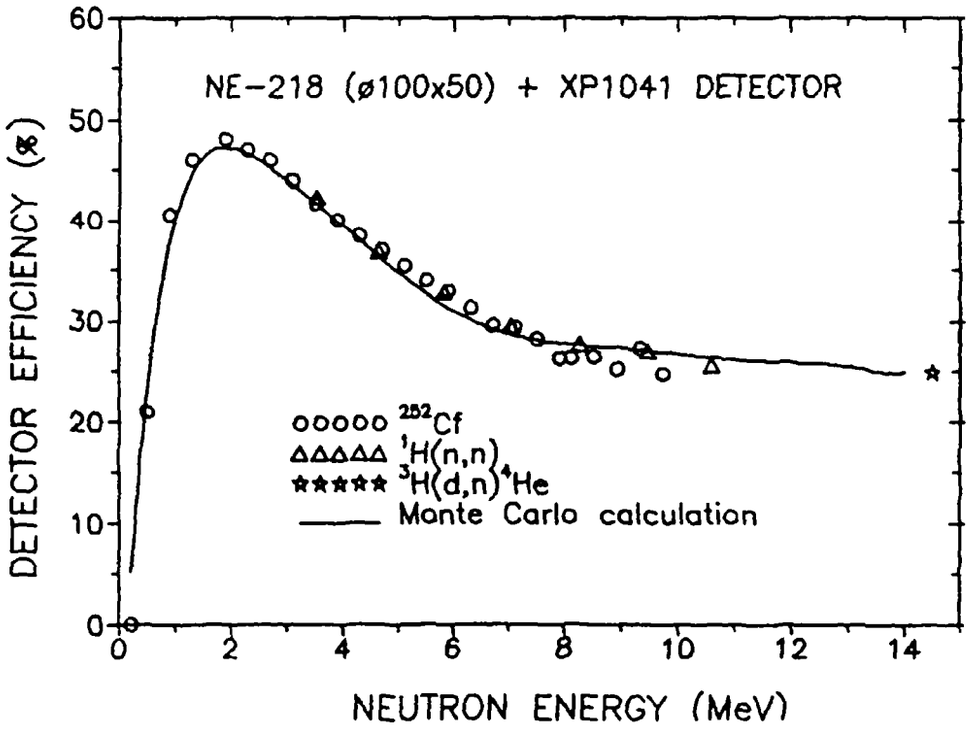

Fig. 2. Efficiency of the neutron detector.

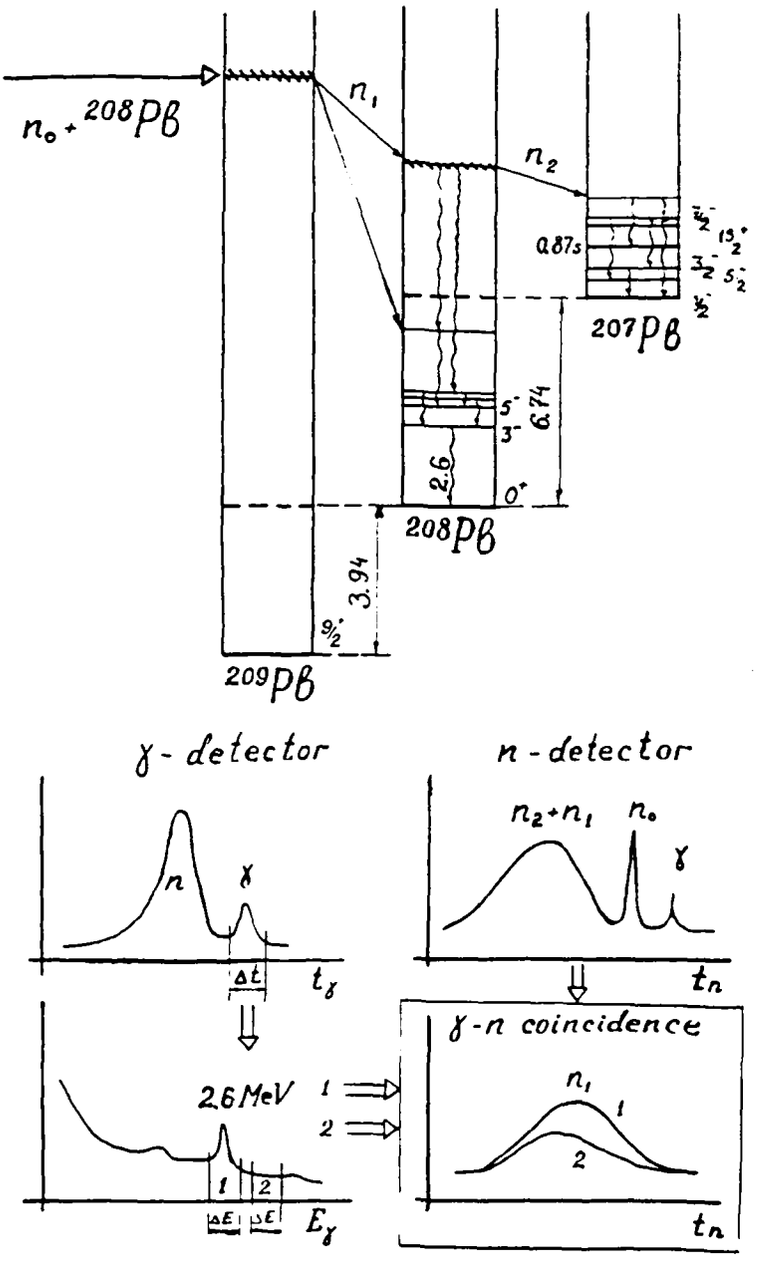

Fig. 3. The idea of $^{208}Pb(n,n'\gamma)$ experiment.

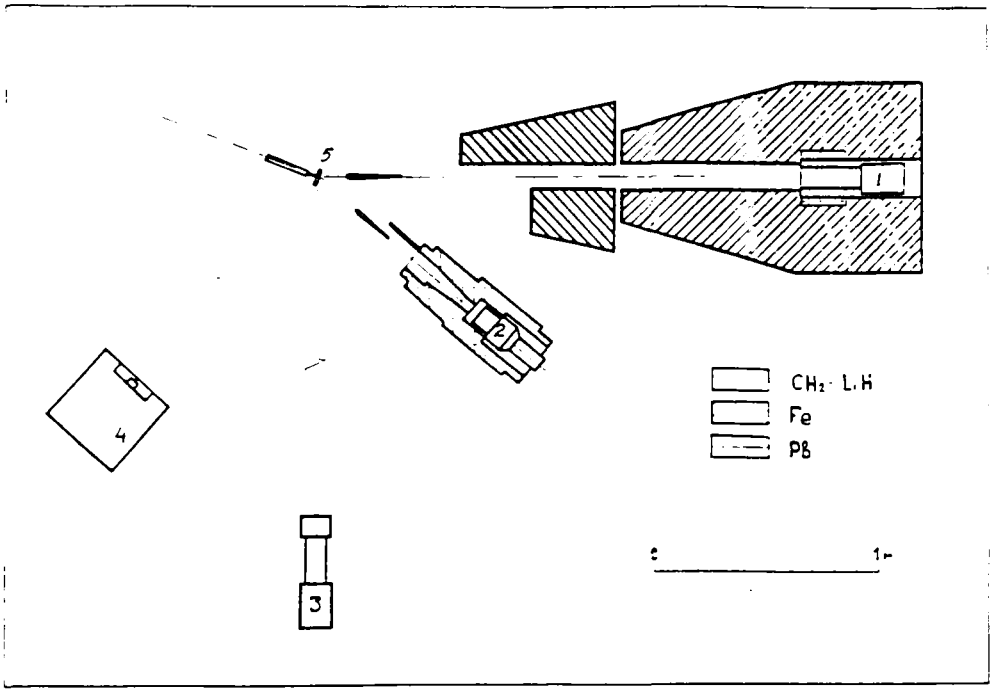

Fig. 4. Lay-out of experiment for measuring the neutron spectra from (n,n'γ) reaction. 1 - neutron detector, 2 - gamma detector, 3 - TOF monitor, 4 - Long Counter, 5 - sample.

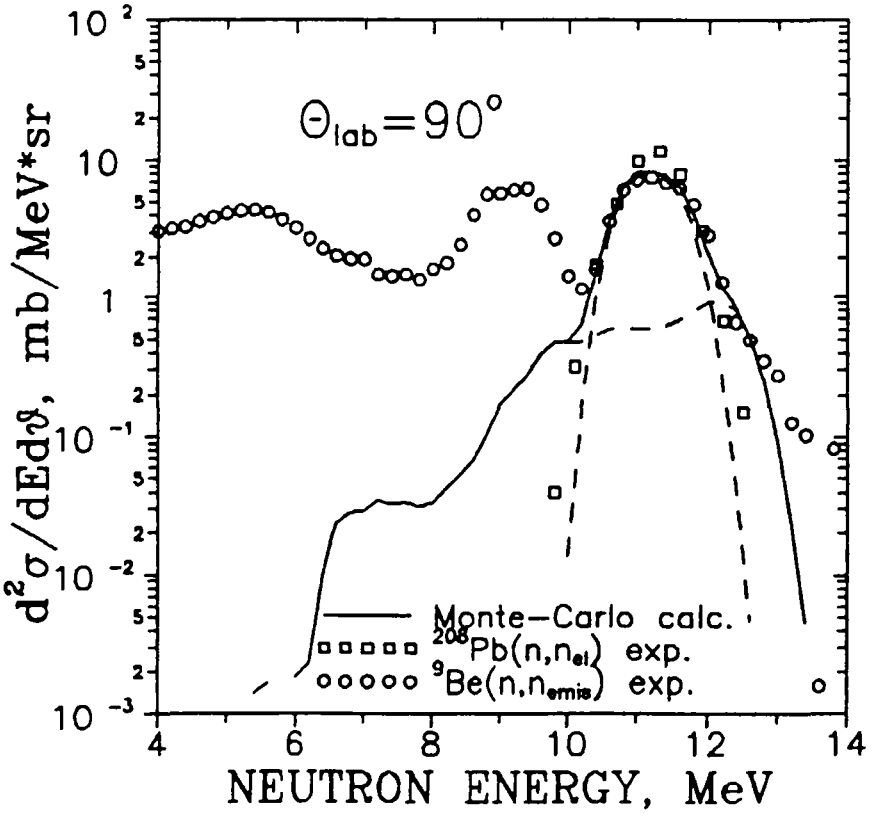

Fig. 5. Elastic peak separation procedure for ^{9}Be at 90 °.

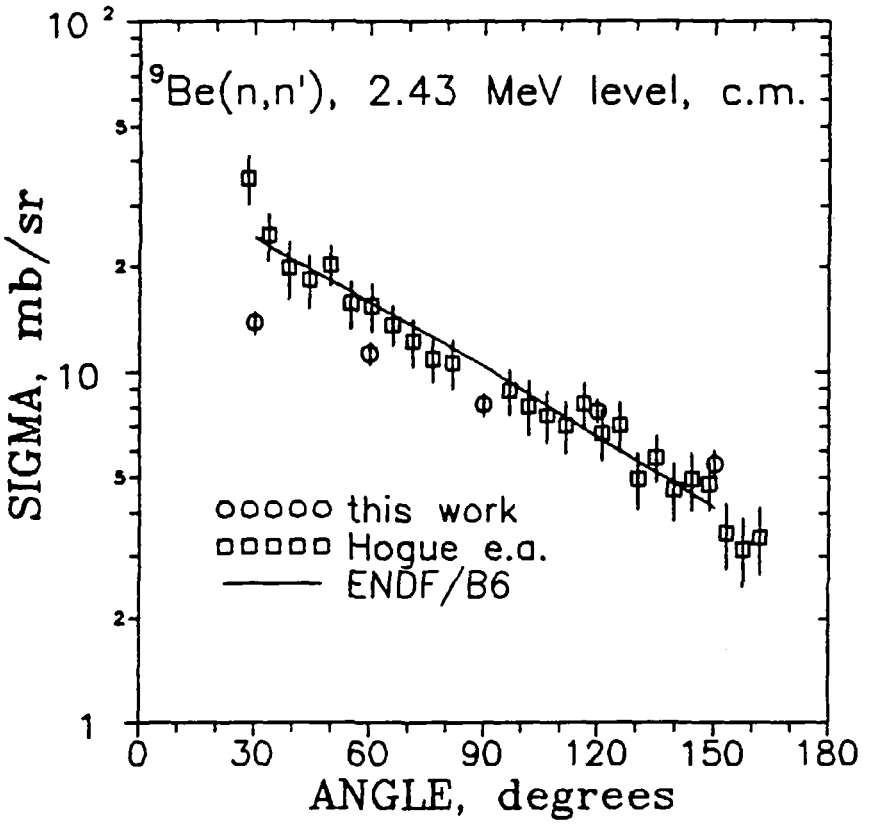

Fig.6. Cross-section of excitation 2.43MeV level in ^{9}Be(n.n') reaction.

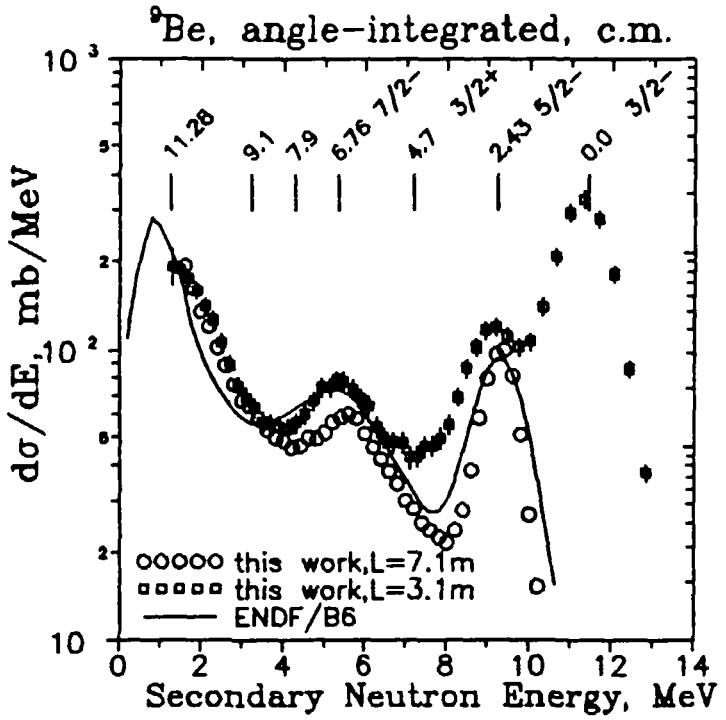

Fig.7. Angle-integrated neutron emission cross-section for ^{9}Be. The arrows indicate the levels of residual ^{9}Be* nucleus.

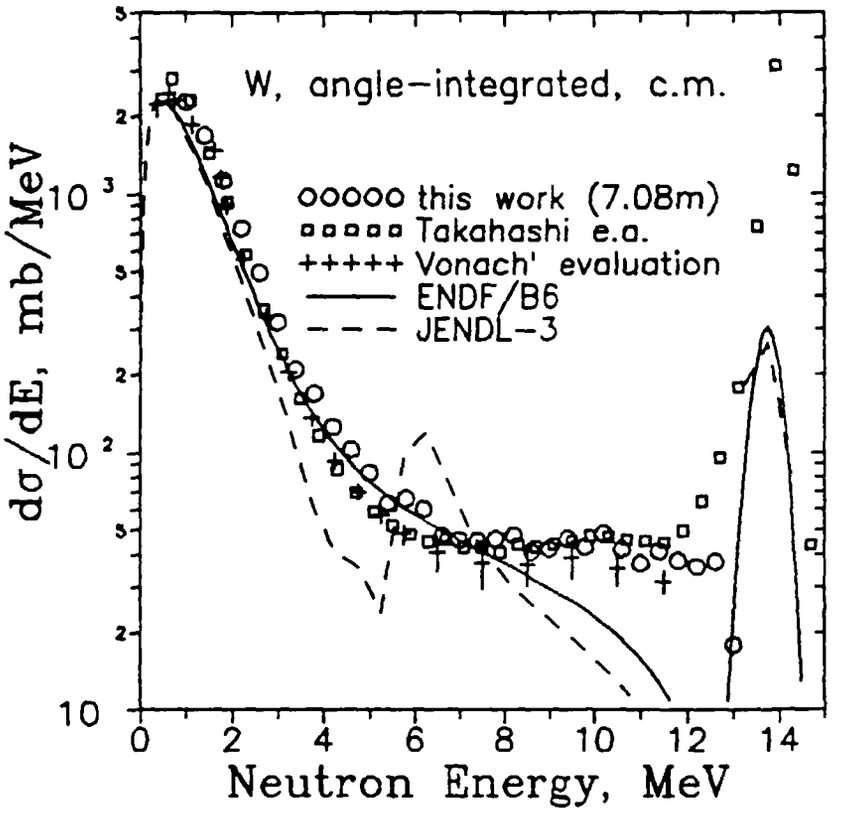

Fig.8. Angle-integrated neutron emission cross-section for W.

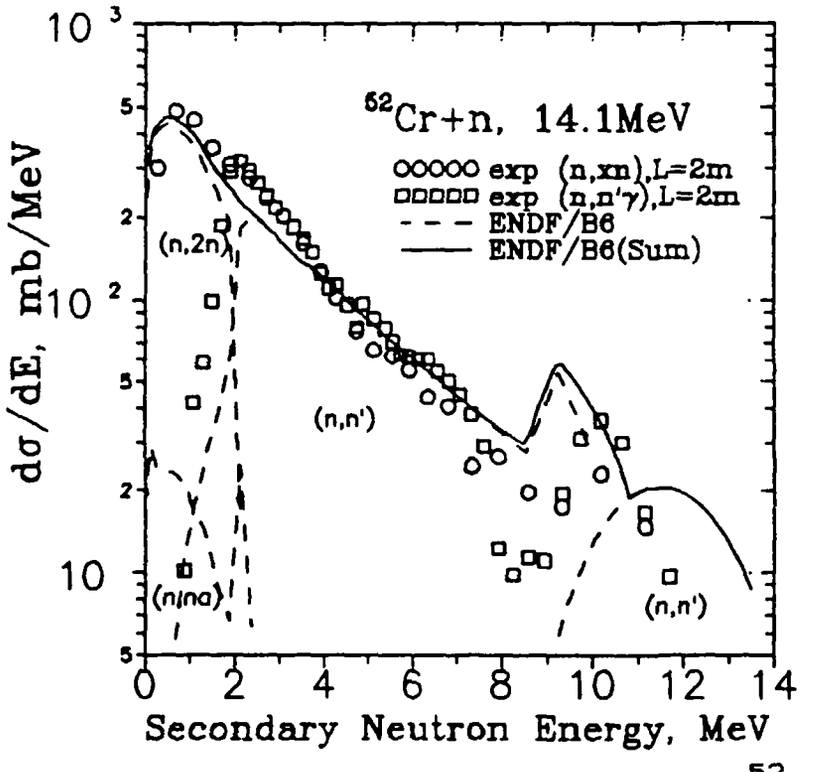

Fig.9. Angle-integrated cross-section for $^{52}Cr(n,xn)$ and $^{52}Cr(n,n'\gamma)$ reactions.

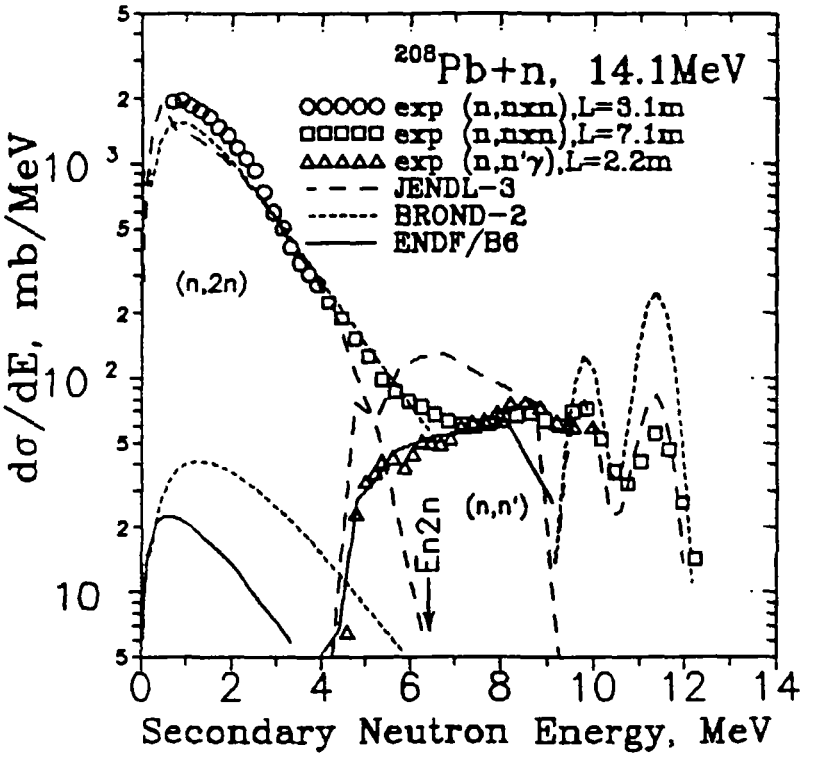

Fig. 10. Angle-integrated cross-section for $^{208}Pb(n,xn)$ and $^{208}Pb(n,n'\gamma)$ reactions.

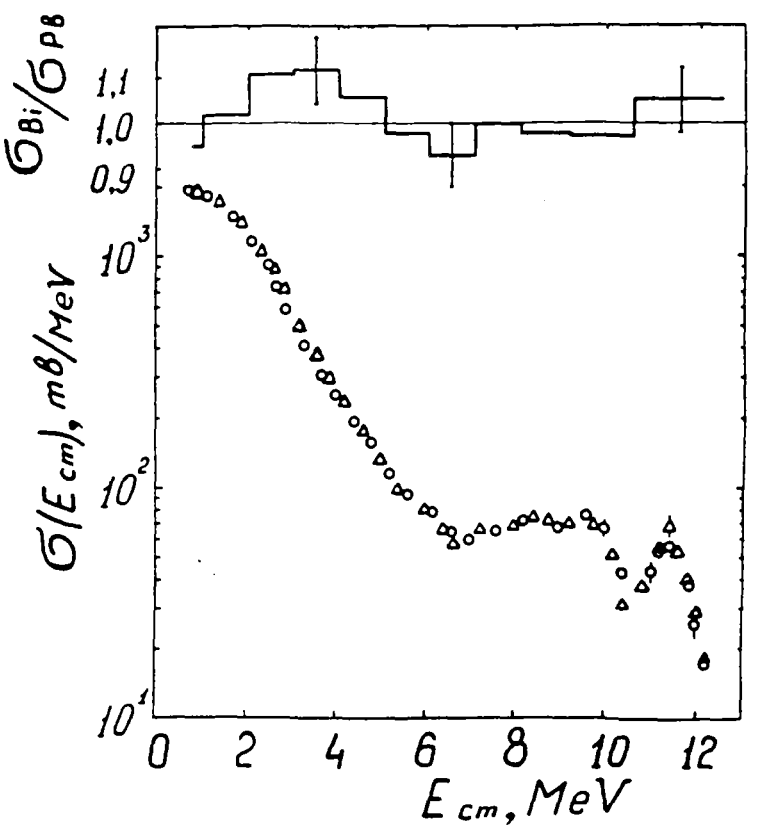

Fig. 11. Angle-integrated neutron emission spectra from 208-Pb(o) and 209-Bi(Δ). In the insert their ratio is shown.

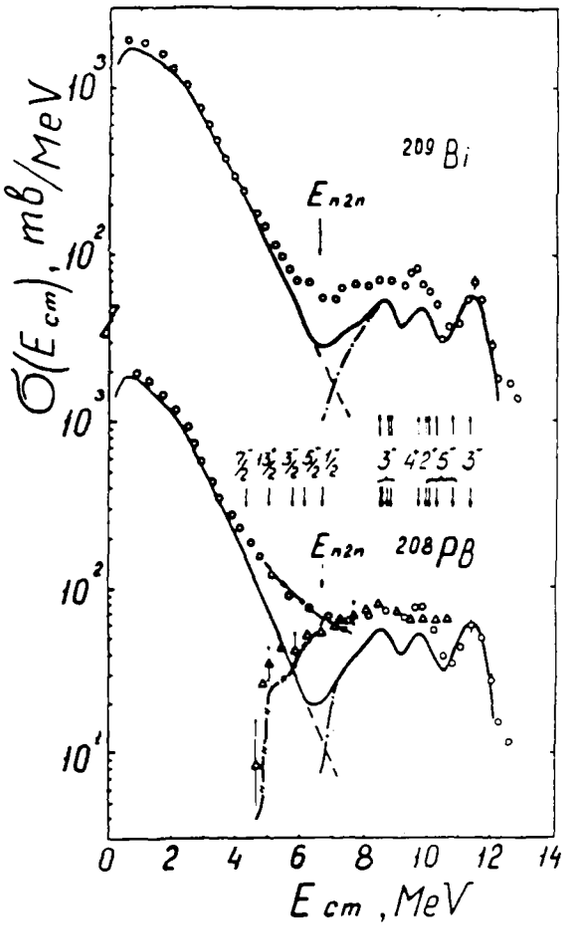

Fig. 12. Comparison of experimental (points) and calculated data
- - - - - compound component,
-.-.- - direct component,
——— - its sum.
-"-"-" - (n, n'γ) spectrum

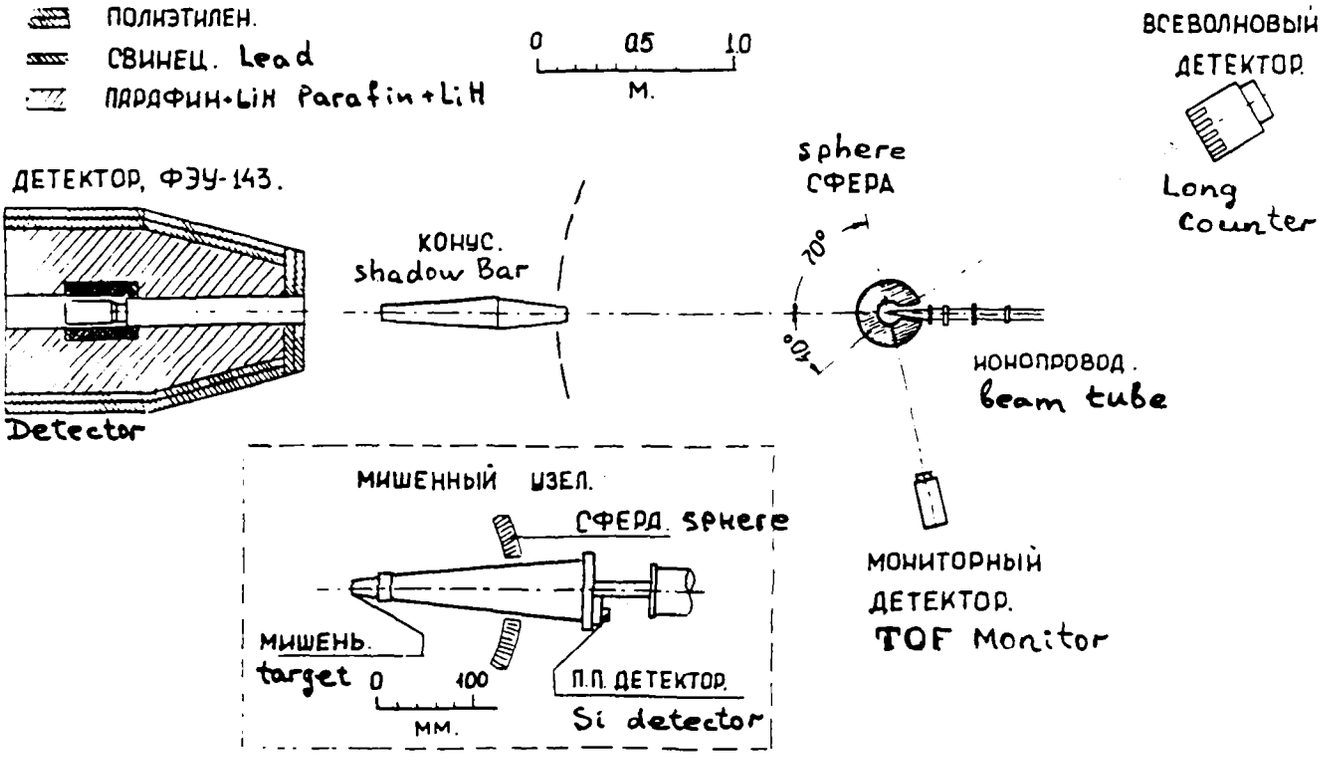

Fig. 13. Benchmark experiment arrangement with T(d, n) source.

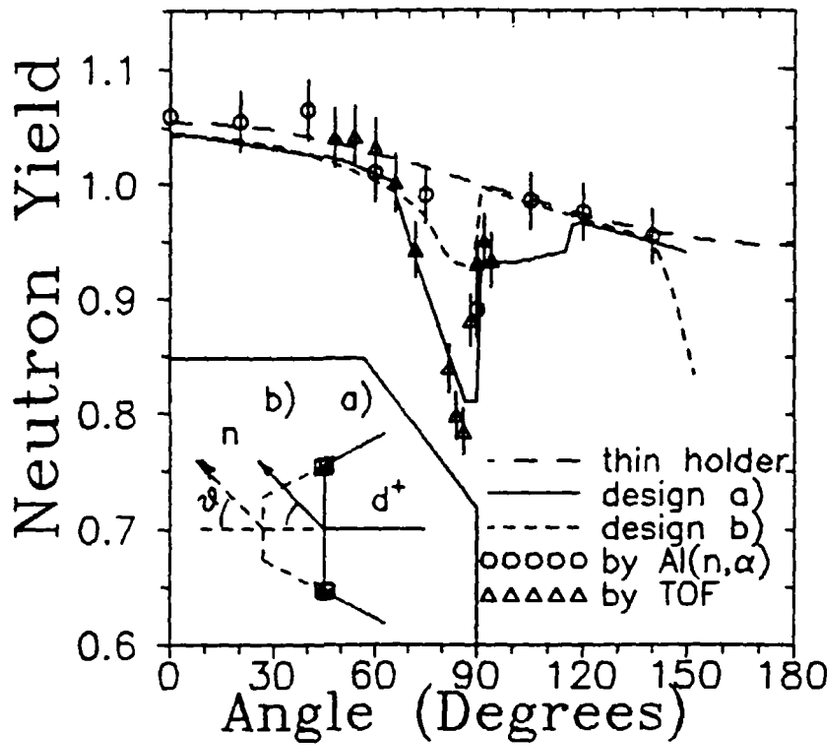

Fig. 14. Angular distribution of 14 MeV neutrons from target assembly, it sketch is shown in the insert.

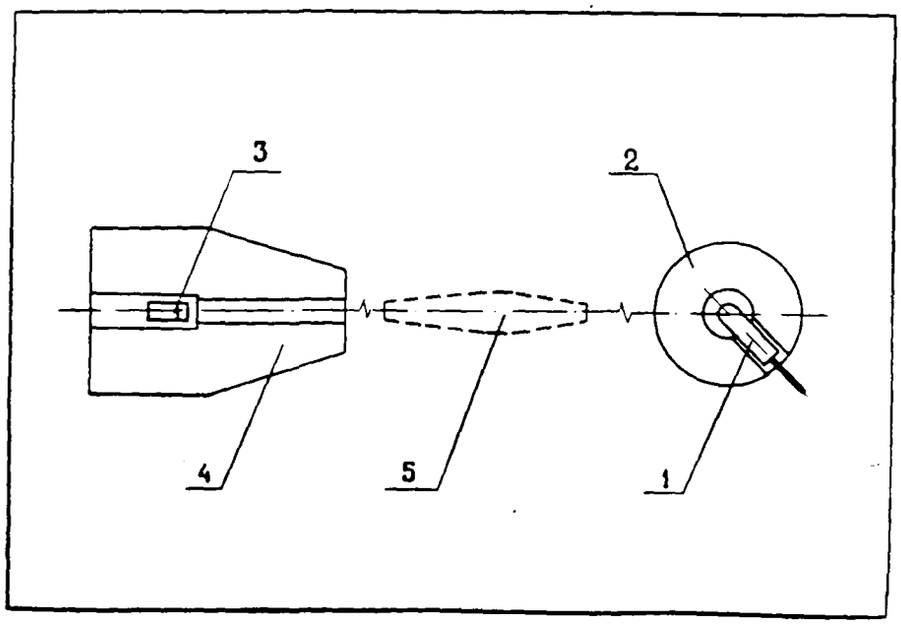

Fig. 15. Benchmark experiment arrangement with ^{252}Cf source.
1 - Cf chamber, 2 - shell, 3 - neutron detector,
4 - detector shield, 5 -shadow bar

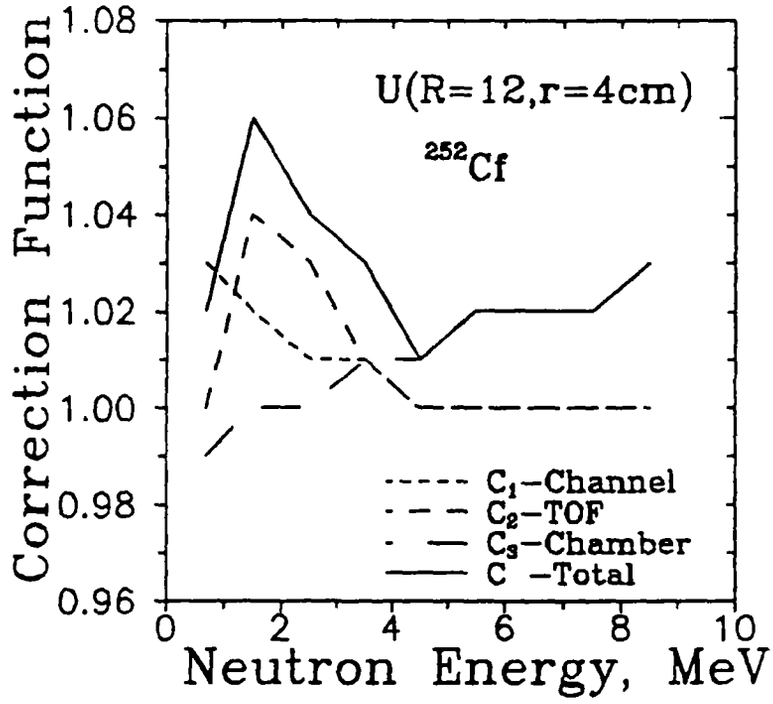

Fig. 16. Correction function for U sphere and ^{252}Cf source.

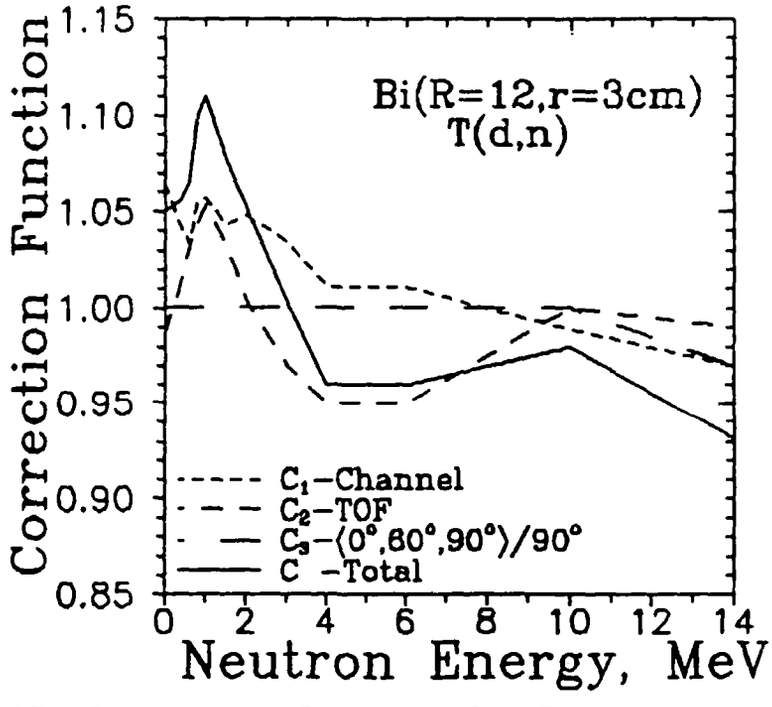

Fig. 17. Correction function for Bi sphere and T(d,n) source.

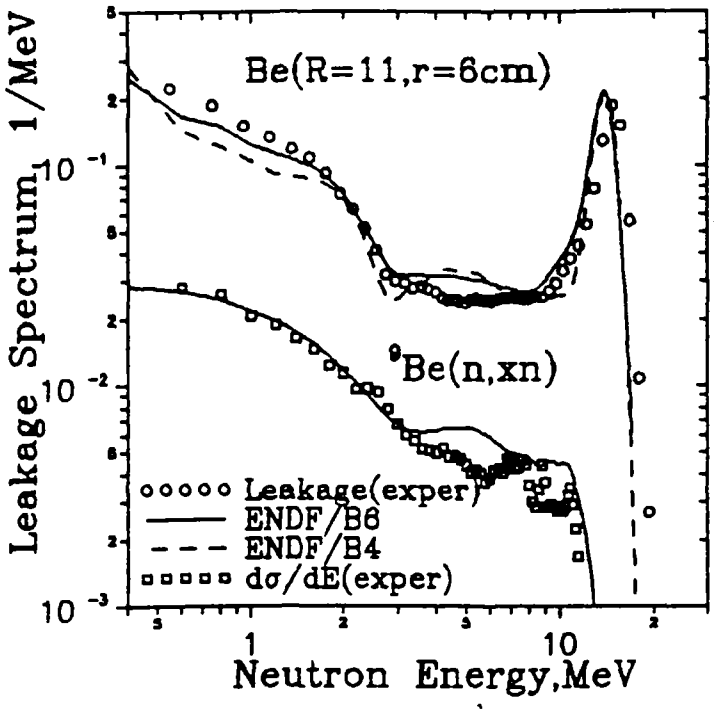

Fig. 18. Leakage neutron spectra from Be sphere with 14MeV source.

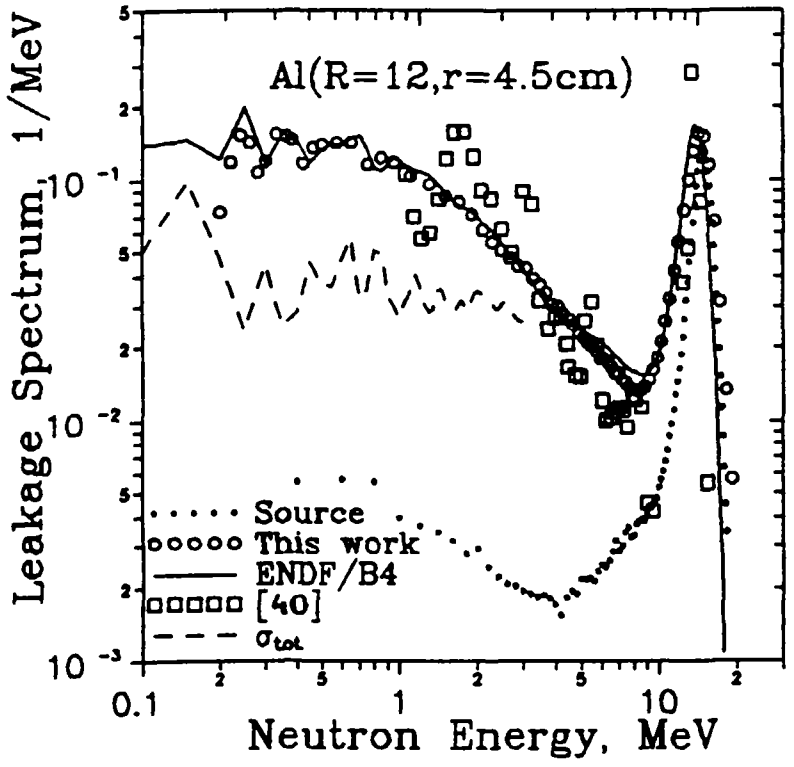

Fig. 19. Leakage neutron spectra from Al sphere with 14MeV source.

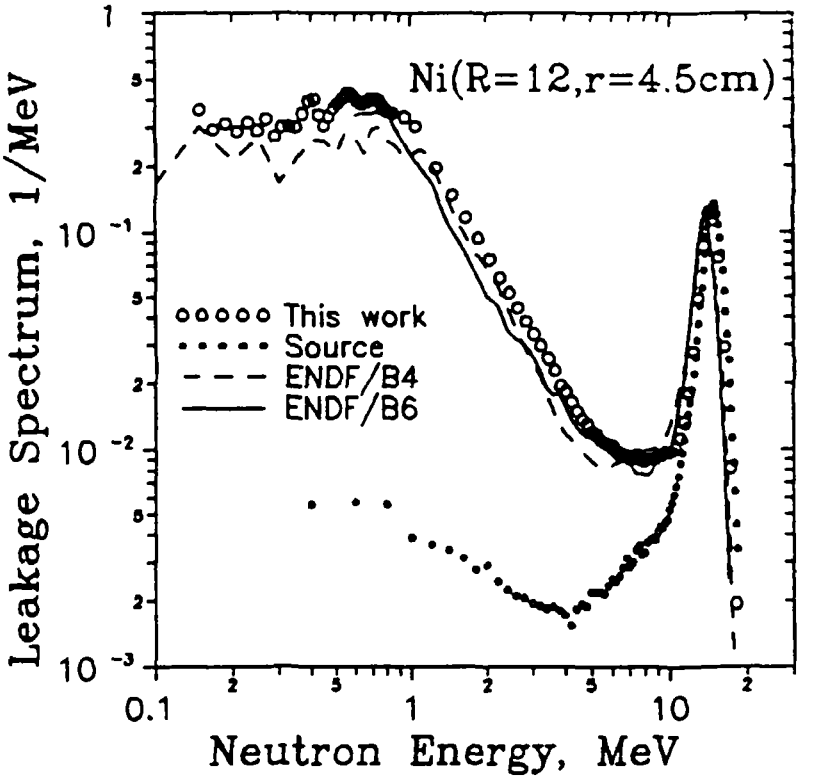

Fig.20. Leakage neutron spectra from Ni sphere with 14MeV source.

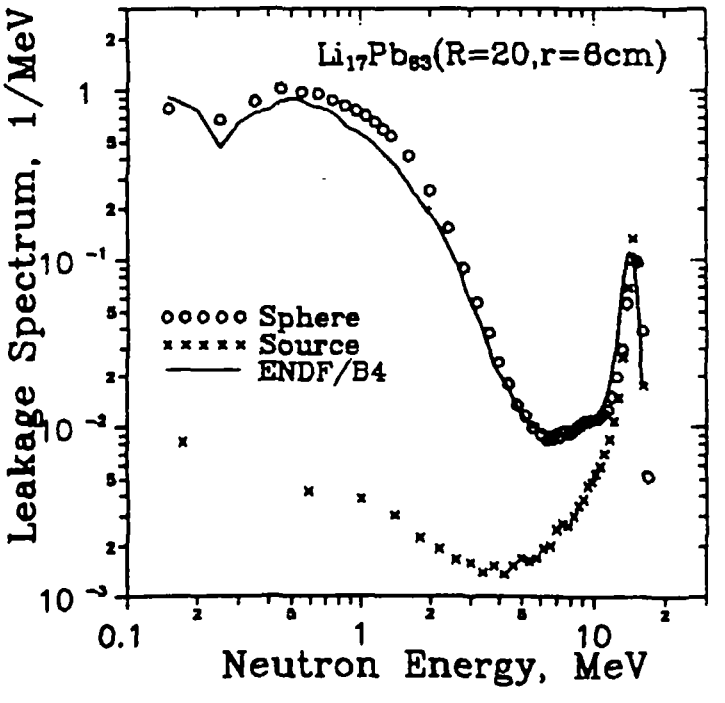

Fig.21. Leakage neutron spectra from LiPb sphere with 14MeV source.

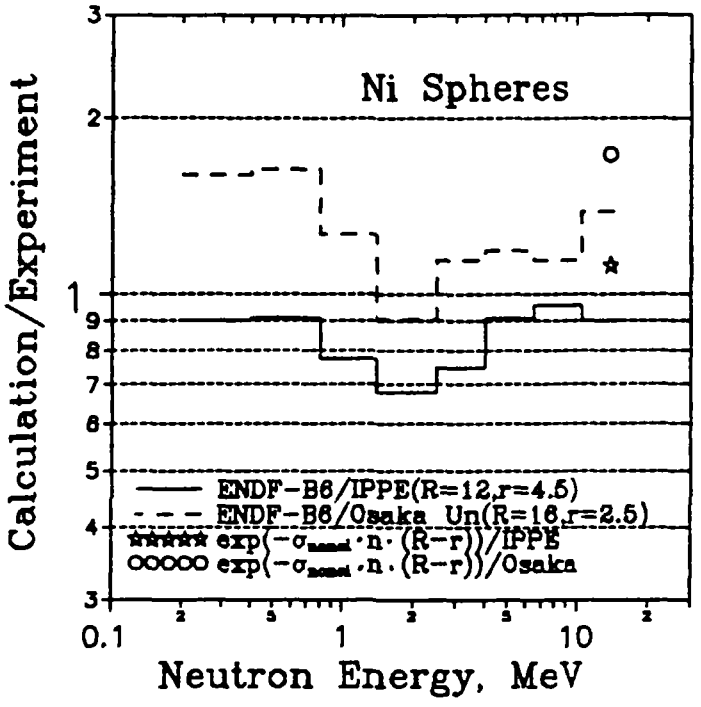

Fig. 22. Ratio of calculated (ENDF/B6) to experimental data (present work and [6]) for Ni spheres.